Computation of stress intensity factors in functionally graded materials using partition-of-unity meshfree method

N. Muthu
IITB-Monash Research Academy, IIT Bombay
Powai, India

S. K. Maiti
Department of Mechanical Engineering, IIT Bombay
Powai, India

B. G. Falzon
brian.falzon@monash.edu
Department of Mechanical and Aerospace Engineering
Monash University
Clayton, Australia

I. Guiamatsia
School of Civil Engineering, The University of Sydney
Sydney, Australia

ABSTRACT

This paper describes the computation of stress intensity factors (SIFs) for cracks in functionally graded materials (FGMs) using an extended element-free Galerkin (XEFG) method. The SIFs are extracted through the crack closure integral (CCI) with a local smoothing technique, non-equilibrium and incompatibility formulations of the interaction integral and the displacement method. The results for mode I and mixed mode case studies are presented and compared with those available in the literature. They are found to be in good agreement where the average absolute error for the CCI with local smoothing, despite its simplicity, yielded a high level of accuracy.

NOMENCLATURE

a	crack length
$\mathbf{a}_I$	jump enriched nodal degree of freedom
$\tilde{a}(\mathbf{x})$	moving least-square unknown constants
$\mathbf{b}_{Ik}$	branch enriched nodal degree of freedom
$\mathbf{B}^{enr}(r,\theta)$	branch enrichment function

Paper No. 3853. Manuscript received 22 June 2012,
revised version received 22 September 2012, accepted 19 October 2012.

https://doi.org/10.1017/S0001924000007636 Published online by Cambridge University Press

C_{ijkl}	material property matrix
d_r	difference range with respect to existing numerical solutions
e	exponential function
e_r	error range with respect to existing theoretical solutions
E	Young's modulus
E_{tip}	Young's modulus at the crack tip.
$f(\mathbf{x})$	signed vector distance function
F	force on the three point bending specimen
$H(f(\mathbf{x}))$	jump function based on $f(\mathbf{x})$
$J(\mathbf{x})$	weighted residual
K_I	Mode I stress intensity factor
K_{II}	Mode II stress intensity factor
K_I^{aux}	auxiliary Mode I stress intensity factor
K_{II}^{aux}	auxiliary Mode II stress intensity factor
L	length of the specimen
M	M-integral/Interaction integral
$p^T(\mathbf{x})$	polynomial basis
q	scalar function for domain integral
r	radial distance from the crack tip
r_c	location behind the crack tip where crack opening displacements are measured
$\mathbf{t}$	traction vector
u_1^{aux}	auxiliary x-displacement
u_2^{aux}	auxiliary y-displacement
$\mathbf{u}_I$	nodal displacement vector
$\mathbf{u}(\mathbf{x})$	actual displacement vector
$\mathbf{u}^a(\mathbf{x})$	approximated displacement vector
$\mathbf{u}_{COD}$	crack opening displacement vector
$\mathbf{u}^-_{COD}$	lower crack face displacement vector
$\mathbf{u}^+_{COD}$	upper crack face displacement vector
U	strain energy density
u	x-displacement field
v	y-displacement field
w	width of the specimen
$w(\mathbf{x})$	weight function
$\mathbf{x}$	sampling point
δ_{ij}	Kronecker delta
ε_{ij}	strain tensor
ε_{ij}^{aux}	auxiliary strain tensor
Δa	virtual crack extension length
Γ	external boundary of the geometry
Γ_{c-}	lower crack boundary
Γ_{c+}	upper crack boundary
Γ_t	boundary on which tractions are prescribed
Γ_u	boundary on which displacements are prescribed
$\Phi_I(\mathbf{x})$	nodal shape functions
κ	Kolosov's constant
μ	shear modulus

https://doi.org/10.1017/S0001924000007636 Published online by Cambridge University Press

θ angle with respect to the local co-ordinate axis at the crack tip
σ_{ij} stress tensor
σ_{ij}^{aux} auxiliary stress tensor
υ Poisson's ratio
υ_{tip} Poisson's ratio at the crack tip
Ω boundary domain

1.0 INTRODUCTION

Functionally graded materials are characterised by spatial changes in the microstructure, resulting in pre-determined gradual changes in the material properties. They have been used as thermal barriers in weight-critical applications, in the nuclear industry and in bio-engineering applications[1-4]. An overview of various aspects of FGMs, with special emphasis on their fracture behaviour, is presented in Ref. 5. FGMs have a heterogeneous microstructure with no sharp discontinuity in material properties. Failure is often due to cracks originating and propagating from inclusions and voids. In this paper, we focus on the numerical modelling of stationary cracks in FGMs.

The finite element method (FEM) has been extensively used for modelling damage in FGMs[6-8]. However the FEM involves extensive re-meshing for crack propagation studies which is computationally costly. This has provided the impetus for the development of the eXtended finite element method (XFEM)[9] and meshfree methods (MMs)[10]. Comi *et al*[11] used the XFEM to study the evolution of cracks in FGMs. This method consists of partition-of-unity enrichment functions to accurately reproduce the displacement field near the crack tip. Motivated by the XFEM, the partition-of-unity concept was adopted in the element-free Galerkin (EFG)[12] method giving rise to the XEFG method[13]. Over the past decade, MMs have been utilised to study the behavior of FGMs[14-15]. Rao *et al*[16] used the EFG method to obtain the SIFs in FGMs with a crack.

Delale *et al*[17] stated that the nature of crack tip asymptotic solutions, in non-homogenous material with continuous and differentiable material properties, was identical to that of a solution in a homogenous material. Erdogan[18] stated that the square root nature of the stress singularity exists at the crack tip in a non-homogeneous medium with smoothly varying elastic properties. Furthermore, Eischen[19] examined mixed-mode cases in non-homogeneous materials using the FEM and confirmed the existence of square root singularity of the stress field ahead of the crack tip. In the light of the above assertions, it is sufficient to locally enrich the region around the crack tip embedded in a non-homogenous medium with that of homogenous crack tip solutions.

The SIF is an important parameter that helps in assessing the resistance of the material to crack propagation. Although there are a variety of techniques available in the FEM and the boundary element method (BEM), e.g., including the displacement method[20], stress method[21], J-integral[22] and CCI[23-25] method, to extract the SIFs, only a few find adoption in MMs. In the FEM, the displacement method and stress method are simple but the SIF obtained depends significantly on the density of the mesh. The most commonly used technique in MMs is the M-integral/interaction integral[26] which is based on the J-integral. Kim *et al*[27], detailed the three independent formulations of the interaction integral for FGMs: 'non-equilibrium', 'incompatibility' and 'constant-constitutive-tensor'. These three differ in the way extra terms are added to counterbalance the difference arising due to the response between homogenous and non-homogenous materials. The first two formulations are simpler and more accurate than the third because they do not involve the derivative of the numerical strain fields.

Non-meshfree techniques based on the CCI[28-29], such as auxiliary FE zone construction and high stiffness spring insertion at the crack tip have been used in MMs. In this paper, we apply a method

https://doi.org/10.1017/S0001924000007636 Published online by Cambridge University Press

that exploits the benefits of both the CCI and MMs to extract the SIFs. The displacement and stress fields, near the crack tip, are modelled using this method and the SIFs are extracted based on Irwin's CCI. In MMs, it is rather easy to get the traction field along a radial direction from the crack tip. The crack opening displacement (COD), which is an important parameter in fracture mechanics, can be obtained from the crack face nodal displacement differences. In XEFG, it is instead obtained from the enrichment functions. The strain energy release rate (SERR) can then be easily calculated from the displacement and traction fields.

The outline of the paper is as follows: The XEFG formulation is detailed in Section 2. In Section 3, the CCI, in conjunction with a local smoothing technique to extract the SIFs is presented. Additionally the interaction integral formulations for FGMs and the displacement method are discussed in brief. In Section 4, two dimensional case studies are examined using the proposed technique and the results obtained are compared with those available in the literature. This is followed by concluding remarks in Section 5.

2.0 DISCONTINUITY MODELLING USING XEFG METHOD

2.1 XEFG method

The moving least squares (MLS) technique[30] is used in the derivation of the shape functions in the EFG method. Any field function $u(\mathbf{x})$ in the MLS technique can be represented by the approximation, $\mathbf{u}^{\mathrm{a}}(\mathbf{x})$, as

$$\mathbf{u}^{\mathrm{a}}(\mathbf{x})=\sum_{i=1}^{m} p_i^{\mathrm{T}}(\mathbf{x})\tilde{a}_i(\mathbf{x}) \qquad \ldots (1)$$

where $p^T(\mathbf{x})$ is the complete polynomial basis and $\tilde{a}(\mathbf{x})$ are the unknown constants. A linear polynomial basis $p^T(\mathbf{x}) = \{1,x,y\}$ is used in this paper.

The unknown $\tilde{a}(\mathbf{x})$ are determined by minimising the weighted residual, $J(\mathbf{x})$, given by

$$\mathrm{J}(\mathbf{x})=\sum_{I=1}^{n} \mathrm{w}_I(\mathbf{x})[p^{\mathrm{T}}(\mathbf{x}_I)\tilde{a}(\mathbf{x})-\mathbf{u}_I]^2 \qquad \ldots (2)$$

where $w_I(\mathbf{x})$ is the weight function, or kernel function, associated with node I. $\mathbf{u}_I$ is the nodal field value. n is the total number of nodes that influences the point $\mathbf{x}$.

The nodes in MMs interact with each other through the weight functions which are user defined and usually have a bell-shaped distribution. Figure 1 shows a domain $\Omega \in R^2$ discretised with nodes associated with circular weight functions.

Minimisation of the residual $J(\mathbf{x})$ in Equation (2) gives

$$A(\mathbf{x})\tilde{a}(\mathbf{x}) = B(\mathbf{x})\mathbf{u}_I \qquad \ldots (3)$$

where $A(\mathbf{x})$ is the moment matrix. $A(\mathbf{x})$ and $B(\mathbf{x})$ are given by,

$$A(\mathbf{x})=\mathrm{w}(\mathbf{x}-\mathbf{x}_I)p(\mathbf{x}_I)p^{\mathrm{T}}(\mathbf{x}_I) \qquad \ldots (4)$$

$$B(\mathbf{x}) = [\mathrm{w}_1(\mathbf{x}-\mathbf{x}_1)p(\mathbf{x}_1),\ldots,\mathrm{w}_i(\mathbf{x}-\mathbf{x}_i)p(\mathbf{x}_i),\ldots,\mathrm{w}_n(\mathbf{x}-\mathbf{x}_n)p(\mathbf{x}_n)] \qquad \ldots (5)$$

A cubic B-spline with a circular domain of influence is used as the weight function. The expression for $\tilde{a}(\mathbf{x})$ is substituted into Equation (1) to obtain the approximated field value in terms of the shape functions.

https://doi.org/10.1017/S0001924000007636 Published online by Cambridge University Press

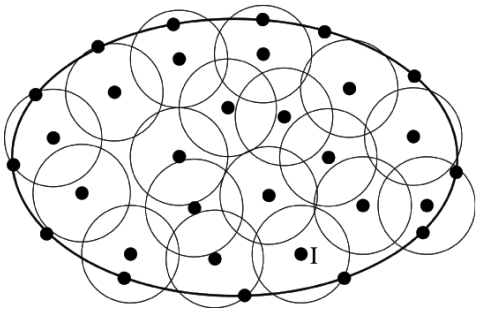


Figure 1. Nodes with their circular weight function.

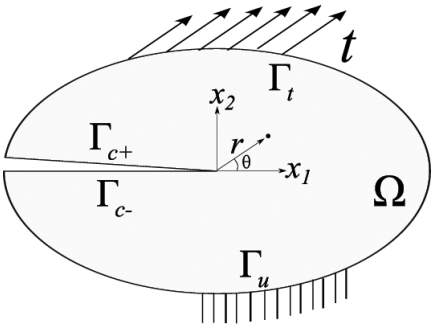


Figure 2. Cracked domain subjected to displacement and traction constraints.

$$\mathbf{u}(\mathbf{x}) = \sum_{I=1}^{n} \Phi_I(\mathbf{x})\mathbf{u}_I \qquad \ldots (6)$$

where $\Phi_I(\mathbf{x})$ is the nodal shape function. The shape functions $\Phi_I(\mathbf{x})$ in Equation (6) are approximants not interpolants. The expression for the shape function is given by:

$$\Phi_I(\mathbf{x}) = p^{\mathrm{T}}(\mathbf{x}).[A(\mathbf{x})]^{-1}.B(\mathbf{x}_I) \qquad \ldots (7)$$

Figure 2 shows a crack, described by Γ_c ($\Gamma_{c+} \cup \Gamma_{c-}$), inside a body. The body is subjected to displacement constraints $\bar{\mathbf{u}}$ on Γ_u of the boundary. Traction $\bar{\mathbf{t}}$ is applied on Γ_t of the boundary.

The displacement approximation[13] in the XEFG method is

$$\mathbf{u}^a(\mathbf{x}) = \sum_{I\in w(\mathbf{x})} \Phi_I(\mathbf{x})\mathbf{u}_I + \sum_{I\in w_j(\mathbf{x})} \Phi_I(\mathbf{x})\{\mathbf{a}_I \mathrm{H}(f(\mathbf{x}))\} + \sum_{I\in w_b(\mathbf{x})} \Phi_I(\mathbf{x}) \sum_{k=1}^{4} \mathbf{b}_{Ik}\mathbf{B}_k^{\mathrm{enr}}(r,\theta) \qquad \ldots (8)$$

where $f(\mathbf{x})$ is the signed distance function from the crack line. The set w includes all the nodes that influences a generic point $\mathbf{x}$, w_b includes the nodes that are branch enriched and w_j includes the nodes that are jump enriched. The normal, jump and branch enriched nodes are shown in Fig. 3.

The Heaviside/jump enriched function $H(f(\mathbf{x}))$ and branch enriched function $\mathbf{B}^{enr}(r,\theta)$ are given by

$$H(f(\mathbf{x})) = \begin{array}{ll} 1 & \text{if } f(\mathbf{x}) \geq 0 \\ -1 & \text{if } f(\mathbf{x}) < 0 \end{array}$$
$$\mathbf{B}^{enr}(r,\theta) = \left[\sqrt{r}\,\mathrm{Sin}\frac{\theta}{2}, \sqrt{r}\,\mathrm{Cos}\frac{\theta}{2}, \sqrt{r}\,\mathrm{Sin}\frac{\theta}{2}\mathrm{Sin}\,\theta, \sqrt{r}\,\mathrm{Cos}\frac{\theta}{2}\mathrm{Sin}\,\theta\right] \qquad \ldots (9)$$

where r and θ are polar co-ordinates with respect to the crack tip as shown in Fig. 2. It is to be noted that the local enrichment for FGMs remains the same as that of the enrichment of crack embedded in the homogenous material.

The COD is essential to extract the SIF through the displacement method. The COD in XEFG is expressed in terms of the jump and branch enrichment functions as follows.

https://doi.org/10.1017/S0001924000007636 Published online by Cambridge University Press

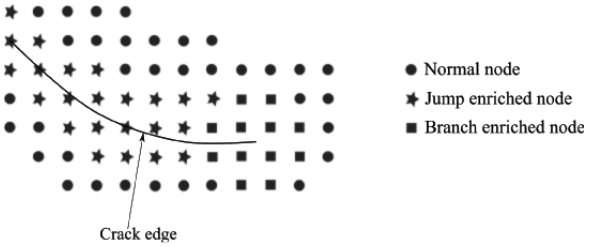


Figure 3. Normal and enriched nodes.

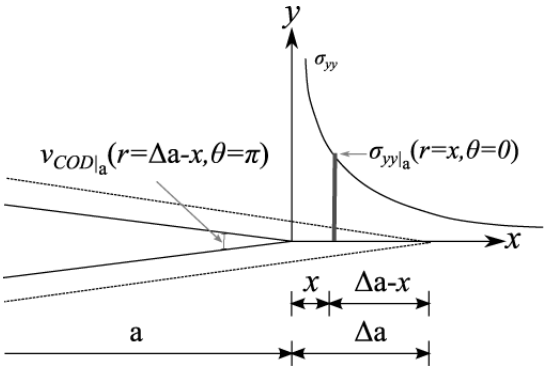


Figure 4. Self similar virtual crack extension.

$$\mathbf{u}_{COD} = \{u_{COD}, v_{COD}\} = \mathbf{u}^{+}_{COD} - \mathbf{u}^{-}_{COD} = 2\left\{\sum_{I\in w_j(\mathbf{x})} \Phi_I(\mathbf{x})\mathbf{a}_I + \sum_{I\in w_b(\mathbf{x})} \Phi_I(\mathbf{x})\sum_{j=1}^{4}\mathbf{b}_{Ij}B_j(r,\pi)\right\} \quad \ldots (10)$$

where $\mathbf{u}^{+}_{COD}$ and $\mathbf{u}^{-}_{COD}$ are the displacement vector of top and bottom face of the crack respectively.

3.0 SIF EXTRACTION TECHNIQUES

3.1 CCI based on local smoothing technique

Figure 4 shows a crack of length a which advances by Δa. For an elastic material, the potential energy released during crack extension is equal to the energy required to close the crack. The potential energy release rate or SERR according to Irwin's CCI is given by

$$G_I = \lim_{\Delta a\to 0}\frac{1}{2\Delta a}\int_0^{\Delta a}\sigma_{yy}v_{COD}\mathrm{d}x$$
$$G_{II} = \lim_{\Delta a\to 0}\frac{1}{2\Delta a}\int_0^{\Delta a}\tau_{xy}u_{COD}\mathrm{d}x \quad \ldots (11)$$

where G_I and G_{II} are Mode I and Mode II energy release rates.

In the local smoothing technique, the approximated displacements and tractions are smoothed over the virtual crack extension length, Δa. These smoothed variations are then substituted in Equation (11) to obtain the SERR.

https://doi.org/10.1017/S0001924000007636 Published online by Cambridge University Press

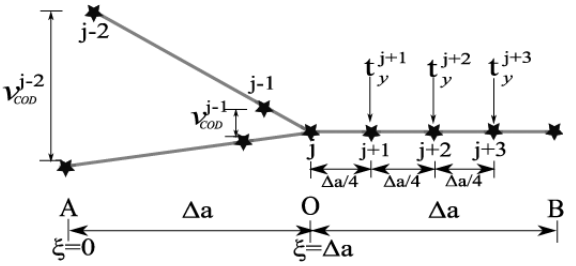


Figure 5. Locations at which displacements and tractions are computed for mode I SIF.

The crack opening displacements are assumed to vary as a function of $\sqrt{x}$. Similarly, the tractions t_x and t_y are assumed to vary as a function of $1/\sqrt{x}$. The COD is assumed to vary as

$$\mathbf{u}_{COD} = \mathbf{a}_\mathbf{u} + \mathbf{b}_\mathbf{u} x + \mathbf{c}_\mathbf{u}\sqrt{x/\Delta a}; \begin{matrix} \mathbf{a}_\mathbf{u} = \{a_u, a_v\}^T \\ \mathbf{b}_\mathbf{u} = \{b_u, b_v\}^T \\ \mathbf{c}_\mathbf{u} = \{c_u, c_v\}^T \end{matrix} \quad \ldots (12)$$

where $\mathbf{u}_{COD} = \mathbf{u}^+_{COD} - \mathbf{u}^-_{COD}$. $\mathbf{a}_\mathbf{u}$, $\mathbf{b}_\mathbf{u}$ and $\mathbf{c}_\mathbf{u}$ are constant vectors that depend on the displacement values at j, $j-1$ and $j-2$ points as shown in Fig. 5. The $j-1^{\text{th}}$ and $j-2^{\text{th}}$ points are located at a distance of $\Delta a/4$ and Δa behind the crack tip respectively. Thereby the COD upon substituting x by $\xi - \Delta a$ in the span, Δa, is obtained as follows:

$$\mathbf{u}_{COD} = 2(\mathbf{u}^{j-2}_{COD} - 2\mathbf{u}^{j-1}_{COD})(1-\xi/\Delta a) + (4\mathbf{u}^{j-1}_{COD} - \mathbf{u}^{j-2}_{COD})\sqrt{1-\xi/\Delta a} \quad \ldots (13)$$

The traction field ahead of the crack tip can be assumed to vary as:

$$\mathbf{t} = \mathbf{a}_\mathbf{t} + \frac{\mathbf{b}_\mathbf{t}}{\sqrt{x/\Delta a}} + \mathbf{c}_\mathbf{t}\sqrt{x/\Delta a}; \begin{matrix} \mathbf{a}_\mathbf{t} = \{a_{t_x}, a_{t_y}\}^T \\ \mathbf{b}_\mathbf{t} = \{b_{t_x}, b_{t_y}\}^T \\ \mathbf{c}_\mathbf{t} = \{c_{t_x}, c_{t_y}\}^T \end{matrix} \quad \ldots (14)$$

where $\mathbf{t}$ $\{t_x, t_y\}$. $\mathbf{a}_\mathbf{t}$, $\mathbf{b}_\mathbf{t}$ and $\mathbf{c}_\mathbf{t}$ are constant vectors.

For mode I crack, the unknown constants can be obtained from the computed traction (t_y) at locations: $j+1$, $j+2$ and $j+3$ as shown in Fig. 5.

$$\begin{Bmatrix} a_{t_y} \\ b_{t_y} \\ c_{t_y} \end{Bmatrix} = \begin{bmatrix} 1 & 2 & 1/2 \\ 1 & \sqrt{2} & 1/\sqrt{2} \\ 1 & 2/\sqrt{3} & \sqrt{3}/2 \end{bmatrix}^{-1} \begin{Bmatrix} t_y^{j+1} \\ t_y^{j+2} \\ t_y^{j+3} \end{Bmatrix} \quad \ldots (15)$$

The obtained unknowns in Equation (15) are substituted in (14) to obtain the approximated traction field, t_y. The tractions can be obtained at any three points over Δa. Here we choose the points in such a way that they are equally distributed across the span Δa and not close to the crack tip. The results are not affected significantly by the choice of these points. It may be noted that the traction, $\mathbf{t}$ used, is σ_{yy} and τ_{xy} ahead of the crack tip for mode I and mode II respectively.

The smoothing technique is used to average the traction locally near the crack tip. It smoothens out the traction field and makes the expression of the SIF derivation simple. A similar technique

https://doi.org/10.1017/S0001924000007636 Published online by Cambridge University Press

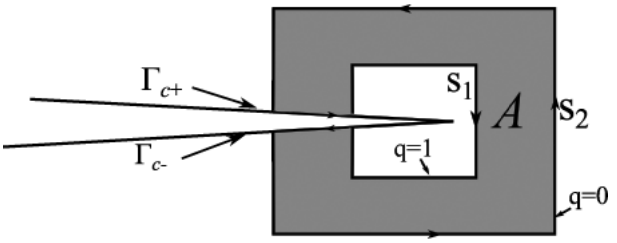


Figure 6. Area for domain integral.

has been used in the context of BEM to obtain the SIFs[31]. On similar lines, once the approximated traction **t** is obtained, it is averaged to obtain the smoothed traction which is given by

$$\mathbf{t}^{avg} = \frac{1}{\Delta a}\int_0^{\Delta a} \mathbf{t}\,dx = (\mathbf{a}_t + 2\mathbf{b}_t + 2/3\mathbf{c}_t) \qquad \ldots (16)$$

To conform to the singularity variation, the local traction is now expressed as follows:

$$\mathbf{t} = \mathbf{t}^{avg}/(2\sqrt{x/\Delta a}) \qquad \ldots (17)$$

The crack closure work done per unit thickness is calculated by substituting Equation (17) and Equation (13) into Equation (11).

$$\begin{aligned} G_I &= \lim_{\Delta a\to 0}\frac{1}{2\Delta a}\int_0^{\Delta a}\sigma_{yy}v_{COD}\,dx \\ G_{II} &= \lim_{\Delta a\to 0}\frac{1}{2\Delta a}\int_0^{\Delta a}\tau_{xy}u_{COD}\,dx \end{aligned} \qquad \ldots (18)$$

Finally the SERR expression for mode I and mode II is given by

$$\begin{aligned} G_I &= 0{\cdot}5\; t_y^{avg}[v_{COD}^{j\text{-}2}(4/3-\pi/4)+v_{COD}^{j-1}(\pi-8/3)] \\ G_{II} &= 0{\cdot}5\; t_x^{avg}[u_{COD}^{j\text{-}2}(4/3-\pi/4)+u_{COD}^{j-1}(\pi-8/3)] \end{aligned} \qquad \ldots (19)$$

A similar expression for G_I and G_{II} for the classical EFG method that has no enrichment is given in Ref. 31.

The CCI is advantageous in MMs as the virtual crack extension length Δa can be set by the user. This Δa is analogous to the crack tip elemental length (OB) in the FEM. The displacement and stress values can be calculated upon fixing Δa. It is worth mentioning that MMs are at an advantage when computing SIFs through the CCI with local smoothing proposed here. Since the MLS shape functions are, at least in theory, smooth, the stress field can be estimated more accurately at a specific location in the domain, as opposed to FEM where the stresses are most accurate at Gauss points.

3.2 Interaction integral for FGMs

Mixed mode SIFs can be effectively calculated through the interaction integral in fracture problems. This integral is based upon the *J*-integral[22] whose domain-based form is given by

https://doi.org/10.1017/S0001924000007636 Published online by Cambridge University Press

$$J = \int_A (\sigma_{ij} u_{i,1} - U\delta_{1j}) q_{,j} \mathrm{d}A + \int_A (\sigma_{ij} u_{i,1} - U\delta_{1j})_{,j} q \mathrm{d}A \quad \ldots (20)$$

where A is the area in Fig. 6 of the domain over which the integral is evaluated. q is a scalar function such that it has a value of unity on S_1 and zero on S_2. The contour S_1 is such that it shrinks to the crack tip while calculating the integral. The strain energy density U is given by

$$U = \frac{1}{2}\sigma_{ij}\varepsilon_{ij} \quad \ldots (21)$$

where σ_{ij} and ε_{ij} are the stress and the strain tensors respectively.

To derive the interaction integral, the actual state and the auxiliary state are superimposed.

$$\begin{aligned} J^s = & \int_A \left\{ (\sigma_{ij} + \sigma_{ij}^{aux})(u_{i,1} + u_{i,1}^{aux}) - \frac{1}{2}(\sigma_{ik} + \sigma_{ik}^{aux})(\varepsilon_{ik} + \varepsilon_{ik}^{aux})\delta_{1j} \right\} q \\ & + \int_A \left\{ (\sigma_{ij} + \sigma_{ij}^{aux})(u_{i,1} + u_{i,1}^{aux}) - \frac{1}{2}(\sigma_{ik} + \sigma_{ik}^{aux})(\varepsilon_{ik} + \varepsilon_{ik}^{aux})\delta_{1j} \right\} \end{aligned} \quad \ldots (22)$$

σ_{ij}^{aux}, ε_{ij}^{aux} and u_1^{aux} are auxiliary state values that corresponds to the theoretical solutions given in Appendix A. Equation (22) can be broken down into three terms: $J^s = \overline{J} + \overline{J}^{aux} + M$. M is called the interaction integral, and is given by

$$\begin{aligned} M = & \int_A (\sigma_{ij} u_{i,1}^{aux} + \sigma_{ij}^{aux} u_{i,1} - \sigma_{ik}\varepsilon_{ik}^{aux}\delta_{1j}) q_{,j} \mathrm{d}A \\ & + \int_A (\sigma_{ij} u_{i,1}^{aux} + \sigma_{ij}^{aux} u_{i,1} - \sigma_{ik}\varepsilon_{ik}^{aux}\delta_{1j})_{,j} q \mathrm{d}A \end{aligned} \quad \ldots (23)$$

Since $(\sigma_{ik}\varepsilon_{ik}^{aux}\delta_{lj})_{,j} = C_{ijkl,l}\varepsilon_{kl}\varepsilon_{ij}^{aux} + \sigma_{ij}^{aux}\varepsilon_{ij,l} + \sigma_{ij}\varepsilon_{ij,l}^{aux}$, the last term of Equation (23) can be further simplified to

$$\begin{aligned} & \int_A (\sigma_{ij} u_{i,l}^{aux} + \sigma_{ij}^{aux} u_{i,l} - \sigma_{ik}\varepsilon_{ik}^{aux}\delta_{lj})_{,j} q \mathrm{d}A = \\ & \int_A (\sigma_{ij,j} u_{i,l}^{aux} + \sigma_{ij} u_{i,lj}^{aux} + \sigma_{ij,j}^{aux} u_{i,l} + \sigma_{ij}^{aux} u_{i,lj}) q \mathrm{d}A \\ & - \int_A (C_{ijkl,l}\varepsilon_{kl}\varepsilon_{ij}^{aux} + \sigma_{ij}^{aux}\varepsilon_{ij,l} + \sigma_{ij}\varepsilon_{ij,l}^{aux}) q \mathrm{d}A \end{aligned} \quad \ldots (24)$$

The non-equilibrium, incompatibility and constant-constitutive-tensor (CCT) formulation depends on the way the second term in the M-integral is simplified[27]. The latter is not discussed here as it requires the derivatives of the actual strain field, which necessitates more computational cost.

3.2.1 Non-equilibrium formulation (M1)

In the non-equilibrium formulation, the actual and auxiliary states satisfy the compatibility condition ($u_{i,lj} = \varepsilon_{ij,l}^{aIx}$, $u_{ij,l}^{au} = \varepsilon_{ij,l}^{aux}$). The actual state satisfies the equilibrium condition ($\sigma_{ij,j} = 0$) but the auxiliary state does not. Therefore Equation (23) can be further simplified into

$$\begin{aligned} M = & \int_A (\sigma_{ij} u_{i,l}^{aux} + \sigma_{ij}^{aux} u_{i,l} - \sigma_{ik}\varepsilon_{ik}^{aux}\delta_{lj}) q_{,j} \mathrm{d}A \\ & + \int_A (\sigma_{ij,j}^{aux} u_{i,l} - C_{ijkl,l}\varepsilon_{kl}\varepsilon_{ij}^{aux}) q \mathrm{d}A \end{aligned} \quad \ldots (25)$$

https://doi.org/10.1017/S0001924000007636 Published online by Cambridge University Press

3.2.2 Incompatibility formulation (M2)

In the incompatibility formulation, the actual state satisfies both the equilibrium ($\sigma_{ij,j} = 0$) and compatibility condition ($u^{aux}_{i,lj} = \varepsilon^{aux}_{ij,l}$) but the auxiliary state satisfies only the equilibrium condition ($\sigma^{aux}_{ij,j} = 0$). Therefore the M-integral becomes

$$M = \int_A (\sigma_{ij} u^{aux}_{i,l} + \sigma^{aux}_{ij} u_{i,l} - \sigma_{ik} \varepsilon^{aux}_{ik} \delta_{lj}) q_j \mathrm{d}A + \int_A (\sigma_{ij} (u^{aux}_{i,lj} - \varepsilon^{aux}_{ij,l}) - C_{ijkl,l} \varepsilon_{kl} \varepsilon^{aux}_{ij}) q \mathrm{d}A \quad \ldots (26)$$

Such a path independent interaction integral given in Equation (26) is derived in Ref. 32.

3.2.3 SIF extraction

The M-integral for a mixed mode problem can be expressed as

$$M = \frac{(2K_I K^{aux}_I + 2K_{II} K^{aux}_{II})}{E^*_{tip}} \quad \ldots (27)$$

where E^*_{tip} is E_{tip} for plane stress and $E_{tip}/(1-\upsilon^2_{tip})$ for plane strain, calculated at the crack tip. K_I is evaluated by setting K^{aux}_I to unity and K^{aux}_{II} to zero. Similarly K_{II} is evaluated by setting K^{aux}_{II} to unity and K^{aux}_I to zero.

3.3 Displacement method

In the displacement method, the COD obtained numerically behind the crack tip is related to the derived theoretical COD solution using linear elastic fracture mechanics (LEFM) assumptions to extract the SIF. The theoretical COD using LEFM for mode I crack can be written as

$$\begin{pmatrix} u_{COD} \\ v_{COD} \end{pmatrix} = \frac{K_I}{2\mu} \sqrt{\frac{r}{2\pi}} \begin{pmatrix} \mathrm{Cos}\frac{\theta}{2}(\kappa - \mathrm{Cos}\,\theta) \\ \mathrm{Sin}\frac{\theta}{2}(\kappa - \mathrm{Cos}\,\theta) \end{pmatrix} \quad \ldots (28)$$

where κ is the Kolosov's constant; $\kappa = 3 - 4\upsilon$ for plane strain and $\kappa = (3 - \upsilon)/(1 + \upsilon)$ for plane stress. μ is the shear modulus.

For K_I, the COD is measured near the crack tip. Generally, it is measured within 5% of crack length, a, behind the crack tip for estimation of mode I SIF. The COD obtained is substituted in Equation (28) to obtain K_I

$$K_I = \frac{2\mu v_{COD|r_c}}{(\kappa+1)} \sqrt{\frac{2\pi}{r_c}} \quad \ldots (29)$$

where r_c is the location behind the crack tip where v_{COD} is evaluated. K_{II} is found following a similar procedure.

4.0 RESULTS

In this section, SIFs are obtained for a number of FGM crack problems using CCI in conjunction with local smoothing. These computed SIFs, along with values computed using other standard methods, are compared with the solutions available in the literature.

https://doi.org/10.1017/S0001924000007636 Published online by Cambridge University Press

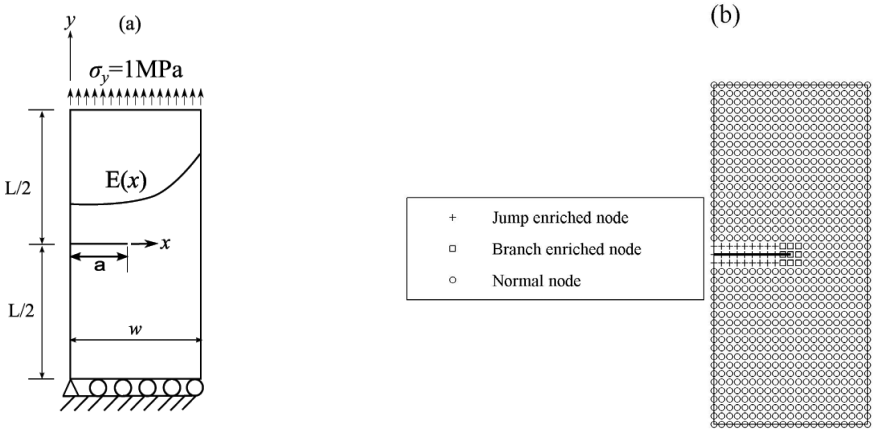


Figure 7. (a) Edge crack subjected to constant tensile traction. (b) Nodal discretisation.

The shape functions of the EFG/XEFG method are non-polynomial in nature. The presence of enrichment terms requires a higher order Gauss quadrature. Therefore the region around the crack was divided into triangular regions to facilitate sub-domain integration. A quadrature rule based on 13th order (i.e., 37 points) is used for the integration near the crack front.

4.1 Mode I edge crack

4.1.1 Constant tensile traction

A plate with dimensions (Fig. 7(a)) w = 1m and L/w = 2 (length-to-width) is subjected to tensile traction (σ_y). The plate is discretised with 21 × 41 regularly distributed nodes as shown in Fig. 7(b) and the domain of influence is set at 1·75 times the nodal spacing.

The elastic modulus varies exponentially, and is given by

$$E(x)=E_I e^{(\eta x)} \quad \ldots (30)$$

where $\eta = ln(E_2/E_1)$, $E_1 = E(0)$ and $E_2 = E(w)$. The value of E_I is 1GPa . Although the elastic modulus varies, the variation in Poisson's ratio (υ) can be considered negligible. Therefore υ is kept constant with a value of 0·3. A plane strain condition is assumed. The crack length a is varied from 0·2 to 0·6. The SIF for each a is calculated with different values of η: 0·1, 0·2, 5 and 10.

The span, Δa, is kept as 0·02a for the CCI calculations. For the CCI without local smoothing, integration of Equation (11) is performed over the span Δa. Sub-domain integration is performed as the displacement and stress vary asymptotically near the crack tip. Δa is divided into 10 sub-domains and five-point Gauss integration is used to evaluate the integral.

In relation to evaluation of the M-integral technique, a square domain with an edge length of 0·25a centred at the crack tip is considered. For the displacement method, the COD is evaluated at 0·02a behind the crack tip.

The SIFs were obtained using five techniques: CCI with local smoothing (CCI-LS), CCI without local smoothing (CCI), M-integral (non-equilibrium formualtion) - M1, M-integral (incompatibility formulation) - M2 and displacement method. Table 4 (Appendix B) shows the

https://doi.org/10.1017/S0001924000007636 Published online by Cambridge University Press

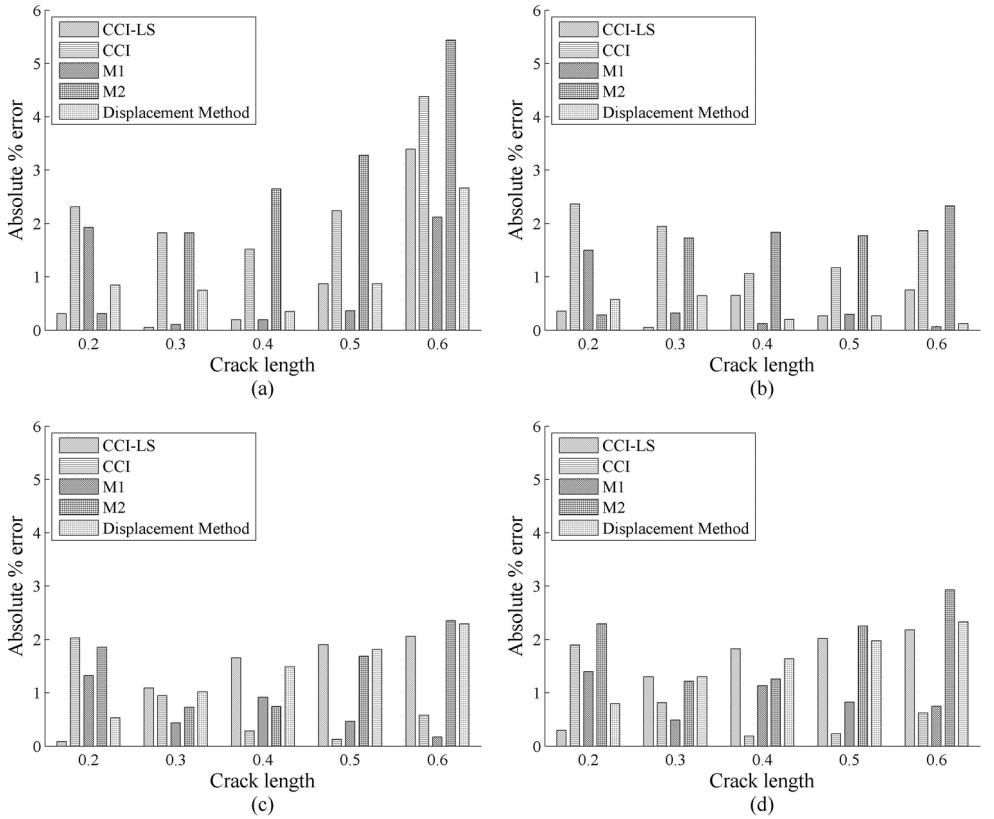


Figure 8. Absolute % error for (a) η = 0·1 (b) η = 0·2 (c) η = 5 (d) η = 10.

normalised mode I SIFs ($K_I / \sigma_y \sqrt{\pi a}$) obtained using different techniques along with the reference results available in the literature.

Figure 8 shows the absolute % error plot for different techniques compared against Ref. [33] results for different values of η. It can be seen that the CCI-LS consistently predicts the mode I SIF with a good level of accuracy, independently of the crack length. It is, generally, as accurate as the M-integral techniques and significantly much simpler.

Table 4 also shows K_I values compared with theoretical result[33]. The CCI without local smoothing has an error range, e_r, of between –4·38% and 0·62%. However, the average error is slightly reduced by applying the local smoothing technique and e_r is between –3·39% and 2·18% by CCI-LS. The following e_r are observed for M1 and M2 integrals: –2·12% to 1·93% and –5·44% to 2·93%. The displacement method has e_r between –2·66% and 2·33%. The errors are indicated immediately below the SIFs and the highest absolute errors are underlined.

4.1.2 Linear tensile traction (Bending load)

The same plate is now subjected to linear traction, as illustrated in Fig. 9. The plate is discretised with 21 × 41 nodes and the domain of influence is again set at 1·75 times the nodal spacing. The elastic modulus varies exponentially as described in Equation (30).

https://doi.org/10.1017/S0001924000007636 Published online by Cambridge University Press

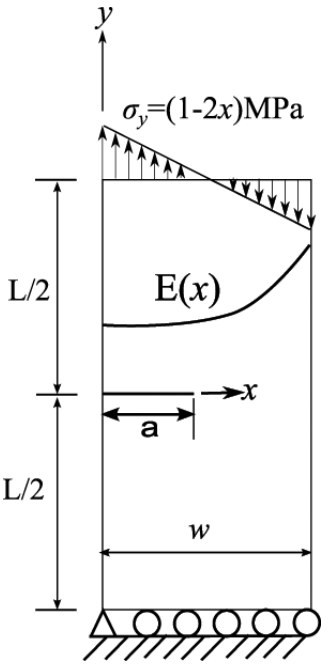


Figure 9. Edge crack subjected to linear tensile traction.

Table 5 (Appendix B) shows K_I for the in-plane bending load. Figure 10 shows the absolute % error plot for different techniques compared against Ref. 33 results for different values of η. This plot is also similar to the ones shown in Fig. 8.

The normalised SIFs ($K_I/(\sigma_{y|x=0}\sqrt{\pi a})$) obtained are compared with Ref. 33. The e_r by CCI-LS and CCI are: –4·97% to 2·60% and –5·82% to 0·95%. The performance of M1 with e_r between –3·90% and 2·48% is better than M2 where the e_r is between –7·14% and 3·01%. The displacement method gives an e_r between –3·09% and 3·13%. The numerical results in Table 4 and Table 5 shows that the SIFs obtained by XEFG method are in good agreement with those in the literature.

4.2 Angle crack in a plate (Mixed mode)

The plate shown in Fig. 11 has a width, w = 1m and a length-to-width ratio, L/w=2 . This plate has an edge crack and is subjected to a traction that varies exponentially. The plate is discretised with 21 × 41 nodes and the domain of influence is set at 1·75 times the nodal spacing.

The crack is oriented at an angle of 45° with respect to the x axis with a normalised crack length of $a/w = 0{\cdot}4\sqrt{2}$. The elastic modulus varies exponentially, and is given by

$$E(x)=\bar{E}e^{(\eta(x-0{\cdot}5))} \quad \ldots (31)$$

$\bar{E}$ is set at 1GPa. η is one of the parameters in Equation (31). The mixed mode SIFs are calculated for the following values of η: 0, 0·1, 0·25, 0·5, 0·75 and 1. A normal stress of magnitude $\sigma_{22} = \bar{\varepsilon}\bar{E}e^{(\eta(x-0{\cdot}5))}$, where $\bar{\varepsilon} = 0{\cdot}001$, is applied on the top boundary of the plate. The υ is kept constant

https://doi.org/10.1017/S0001924000007636 Published online by Cambridge University Press

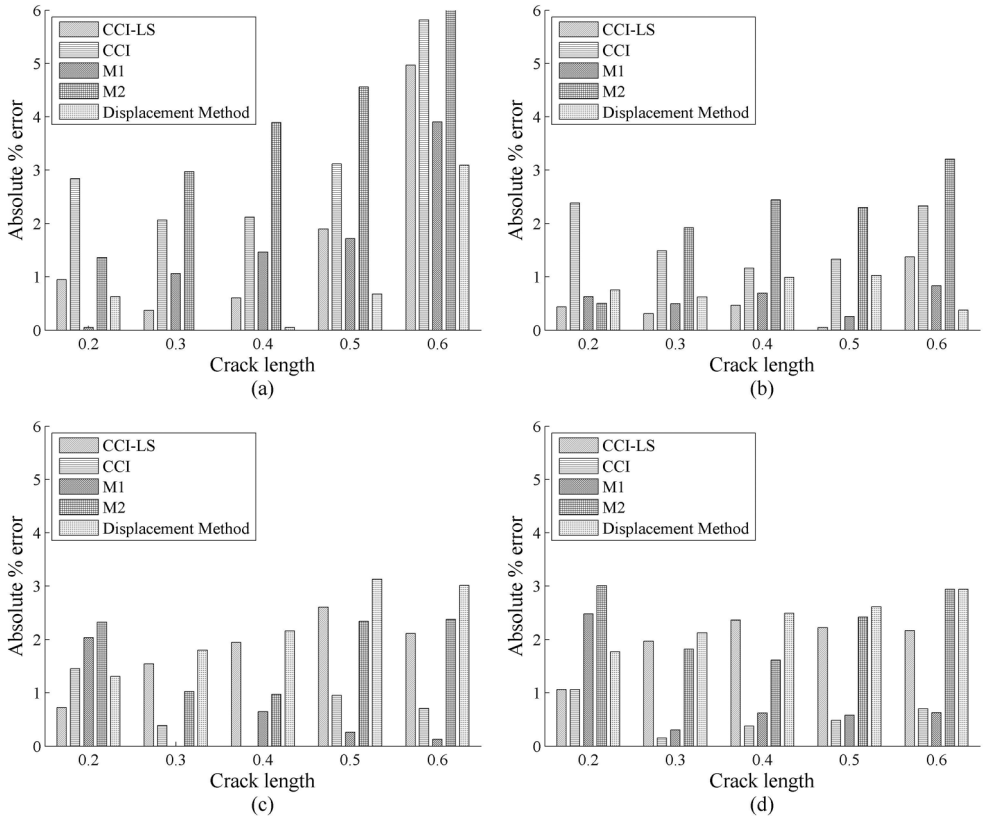


Figure 10. % Absolute error for (a) η = 0·1 (b) η = 0·2 (c) η = 5 (d) η = 10.

with a value of 0·3. A plane strain condition is assumed.

The obtained mode I and II SIFs are normalised with respect to $\bar{\varepsilon}\bar{E}\sqrt{\pi a}$, and are given by.

$$\hat{K}_I = \frac{K_I}{\bar{\varepsilon}\bar{E}\sqrt{\pi a}}$$
$$\hat{K}_{II} = \frac{K_{II}}{\bar{\varepsilon}\bar{E}\sqrt{\pi \mathrm{a}}} \quad \ldots (32)$$

The span, Δa, is kept as $0{\cdot}02a$ for CCI calculations. A square domain with an edge length of $0{\cdot}25a$ centred at the crack tip is used for the M-integral technique. The COD is evaluated at $0{\cdot}02a$ behind the crack tip for the displacement method. Table 1 and Table 2 show the mode I and II SIFs calculated for various η, for a fixed crack length, respectively.

The results are compared with FEM results[8] in the literature. In Table 1, it is observed that the SIF based on CCI results significantly improve by the local smoothing technique. The K_I by CCI without local smoothing has a difference range (d_r) from –8·24% to –8·06%. However, the d_r is significantly reduced to a narrow range between –2·94% and –2·72% by the application of the local smoothing technique. The displacement method gives excellent results with d_r of –0·40% to –0·30%. The following d_r are observed for M1 and M2 integrals: –2·01% to –0·96% and –1·03% to –0·60%.

https://doi.org/10.1017/S0001924000007636 Published online by Cambridge University Press

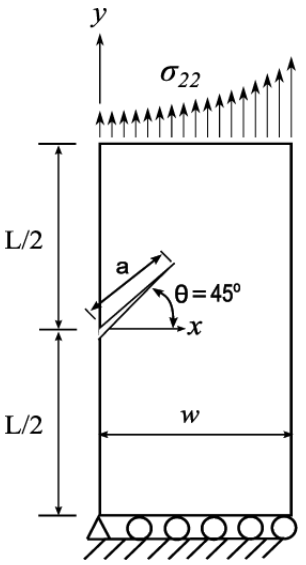


Figure 11. Angle crack under mixed mode.

Table 1
Normalised mode I SIF for angle crack under mixed mode

			Normalised mode I SIF				
η	**Ref. 19**	**Ref. 8**	**CCI-LS**	**CCI**	**M1**	**M2**	**Displacement method**
0·00	1·438	1·451	1·409	1·332	1·437	1·436	1·446
			–2·89%	–8·20%	–0·96%	–1·03%	–0·34%
0·10	-	1·396	1·355	1·281	1·380	1·382	1·391
			–2·94%	–8·24%	–1·15%	–1·00%	–0·36%
0·25	-	1·316	1·279	1·209	1·300	1·304	1·312
			–2·81%	–8·13%	–1·22%	–0·91%	–0·30%
0·50	-	1·196	1·163	1·099	1·178	1·187	1·192
			–2·76%	–8·11%	–1·51%	–0·75%	–0·33%
0·75	-	1·089	1·059	1·001	1·070	1·081	1·085
			–2·75%	–8·08%	–1·74%	–0·73%	–0·37%
1·00	0·984	0·993	0·966	0·913	0·973	0·987	0·989
			–2·72%	–8·06%	–2·01%	–0·60%	–0·40%

Here again in Table 2, the d_r associated with CCI, –6·13% to –5·64%, is significantly reduced to the d_r of –0·35 % to 0·25% by CCI-LS. The performance of M1 and M2 integral is good with d_r of 0·75% to 1·32% and 1·32% to 4·23% respectively. The displacement method has d_r of –1·55% to –1·13%.

https://doi.org/10.1017/S0001924000007636 Published online by Cambridge University Press

Table 2
Normalised mode II SIF for angle crack under mixed mode

	Normalised mode II SIF						
η	Ref. 19	Ref. 8	CCI-LS	CCI	M1	M2	Displacement method
0·00	0·605	0·604	0·602	0·567	0·612	0·612	0·595
			–0·33%	–6·13%	1·32%	1·32%	–1·49%
0·10	-	0·579	0·577	0·544	0·586	0·588	0·570
			–0·35%	–6·04%	1·21%	1·55%	–1·55%
0·25	-	0·544	0·543	0·511	0·550	0·555	0·536
			–0·18%	–6·07%	1·10%	2·02%	–1·47%
0·50	-	0·491	0·490	0·462	0·496	0·505	0·484
			–0·20%	–5·91%	1·02%	2·85%	–1·43%
0·75	-	0·443	0·444	0·418	0·447	0·460	0·438
			0·23%	–5·64%	0·90%	3·84%	–1·13%
1·00	0·395	0·402	0·403	0·379	0·405	0·419	0·397
			0·25%	–5·72%	0·75%	4·23%	–1·24%

Table 3
Normalised mode I SIF for composite strip

	Normalised mode I SIF							
η*a*	Ref. 19 CCT	Ref. 16 M2	Ref. 16 method	CCI-LS	CCI	M1	M2	Displacement
0	2·112	2·133	2·133	2·140	2·100	2·147	2·147	2·133
				0·33%	–1·55%	0·66%	0·66%	0·00%
2	2·295	2·304	2·348	2·321	2·283	2·341	2·316	2·317
				0·74%	–0·91%	1·61%	0·52%	0·56%
4	2·571	2·589	2·670	2·592	2·553	2·633	2·578	2·587
				0·12%	–1·39%	1·70%	–0·42%	–0·08%
6	2·733	2·769	2·879	2·744	2·707	2·811	2·723	2·738
				–0·90%	–2·24%	1·52%	–1·66%	–1·12%
20	3·228	3·314	3·579	3·118	3·093	3·420	3·092	3·113
				–5·91%	–6·67%	3·20%	–6·70%	–6·07%

4.3 Mode I crack in a composite strip

Consider the composite strip with mode I crack as shown in Fig. 12. The strip has dimensions, w =1m (width) and $L/w = 2$ (length-to-width) with an edge crack of $a/w = 0{\cdot}4$.

The υ is kept constant with value 0·3. The elastic modulus is a function of the hyperbolic tangent function, given by

$$E(x)=\frac{E_1+E_2}{2}+\frac{E_1-E_2}{2}\,\mathrm{Tan}\,h(x\eta\text{-}0\cdot4\eta) \qquad \ldots (33)$$

where E_1 =1GPa and E_2/E_1 =3. As η increases, the discontinuity in elastic modulus becomes sharper

https://doi.org/10.1017/S0001924000007636 Published online by Cambridge University Press

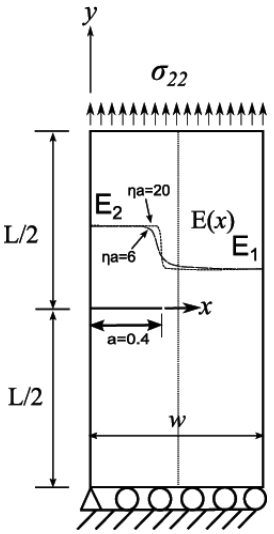


Figure 12. Composite strip with mode I crack.

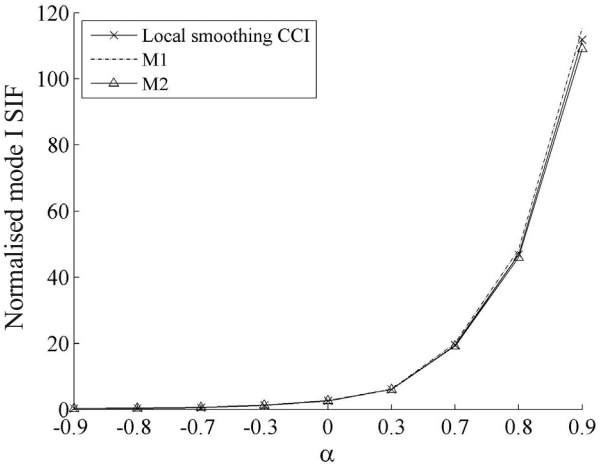


Figure 13. Normalised mode I SIF as a function of the elastic mismatch for $\eta a = 6$.

at the crack tip. A plane strain condition is assumed. A tensile traction of $\sigma_{22} = \bar{\varepsilon}E(x)/(1-\upsilon^2)$, where $\bar{\varepsilon} = 0{\cdot}001$, is applied on the top boundary of the strip to maintain uniform strain.

The composite is discretised with 21×41 nodes and the domain of influence is set at 1·75 times the nodal spacing. Table 3 shows mode I SIFs obtained for different values of ηa.

The span, Δa, is kept as $0{\cdot}02a$ for CCI calculations. A square domain with an edge length of $0{\cdot}01a$ centred at the crack tip is considered for the M-integral technique. The COD is evaluated at $0{\cdot}02a$ behind the crack tip for the displacement method.

Good results are obtained by the XEFG method. The normalised SIF results ($(1-\upsilon^2)\, K_I / \bar{\varepsilon}E(x=0)\sqrt{\pi a}$) are compared with those based on the M-integral's CCT formulation[16]. The following are the e_r of SIFs using various methods: –5·91% to 0·74% by CCI-LS, –6·67% to –0·91% by CCI, 0·66% to 3·20% by M1 integral, –6·70% to 0·66% by M2 integral and –6·07% to 0·56% by displacement method. All the techniques deviate as ηa takes higher value. It may be due to the fact that at higher values the material behaves more like a bi-material.

Dundurs[35] first parameter is introduced (Equation (34)) which takes into effect a number of material parameters.

$$\alpha = \frac{\mu_2(\kappa_1+1) - \mu_1(\kappa_2+1)}{\mu_2(\kappa_1+1) + \mu_1(\kappa_2+1)} \quad \ldots (34)$$

where μ_j is the shear modulus of material with $j = 1$ for material 1 with Young's modulus E_1 and $j = 2$ for material 2 with Young's modulus E_2, and $\kappa_j = 3 - 4\upsilon_j$ under the plane strain condition. As material 1 becomes more complaint compared to material 2, the value of α increases.

Figure 13 shows the mode I SIFs obtained using local smoothing with CCI, M1 and M2 techniques that agree well each other and increase non linearly with α. This implies that the crack in stiffer medium has more probability to penetrate the complaint medium than to deflect along the material interface.

https://doi.org/10.1017/S0001924000007636 Published online by Cambridge University Press

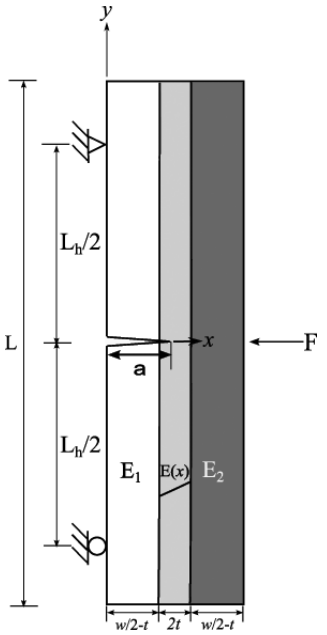


Figure 14. Mode I crack in TPB specimen.

4.4 Three point bending (TPB) specimen with mode I crack

Figure 14 shows a mode I crack embedded inside a TPB specimen. In the horizontal direction, the specimen consists of a FGM layer that is sandwiched between two different homogenous materials. The specimen has dimensions: w = 1m (width) and L/w = 5·4 (length-to-width) with a FGM layer of width ($2t$) 0·1m.

The variation of elastic modulus is assumed as follows.

$$E(x)=\begin{cases} E_2, & x>w/2+t \\ \dfrac{E_1+E_2}{2}+\dfrac{E_2-E_1}{2t}(x-w/2), & w/2-t\le x\le w/2+t \\ E_1, & x<w/2-t \end{cases} \quad \ldots (35)$$

A plane strain condition is assumed. A concentrated load of F = 1MPa is applied, as shown in Fig. 14. The specimen is constrained at two locations that are equidistant from the x-axis such that the ratio, L_h/w = 5. The υ is held constant at 0·3. The value of E_1 is 1GPa.

Three different crack lengths are chosen: a/w = 0·45, 0·5 and 0·55 such that the crack tip is either at the material interface or in the middle of the FGM layer. Normalised mode I SIFs ($K_I\sqrt{w/2}/F$) are obtained for different E_2/E_1 ratios. The specimen is discretised with 21 × 41 nodes and the domain of influence is set at 1·75 times the nodal spacing.

The span, Δa, is kept as 0·005a for CCI calculations. A square domain with an edge length of 0·02a centred at the crack tip is used for the M-integral technique. The COD is evaluated at 0·005a behind the crack tip for the displacement method. Figure 15 shows the absolute % error plot for different techniques compared against Ref. 8 results for different a/w ratios.

https://doi.org/10.1017/S0001924000007636 Published online by Cambridge University Press

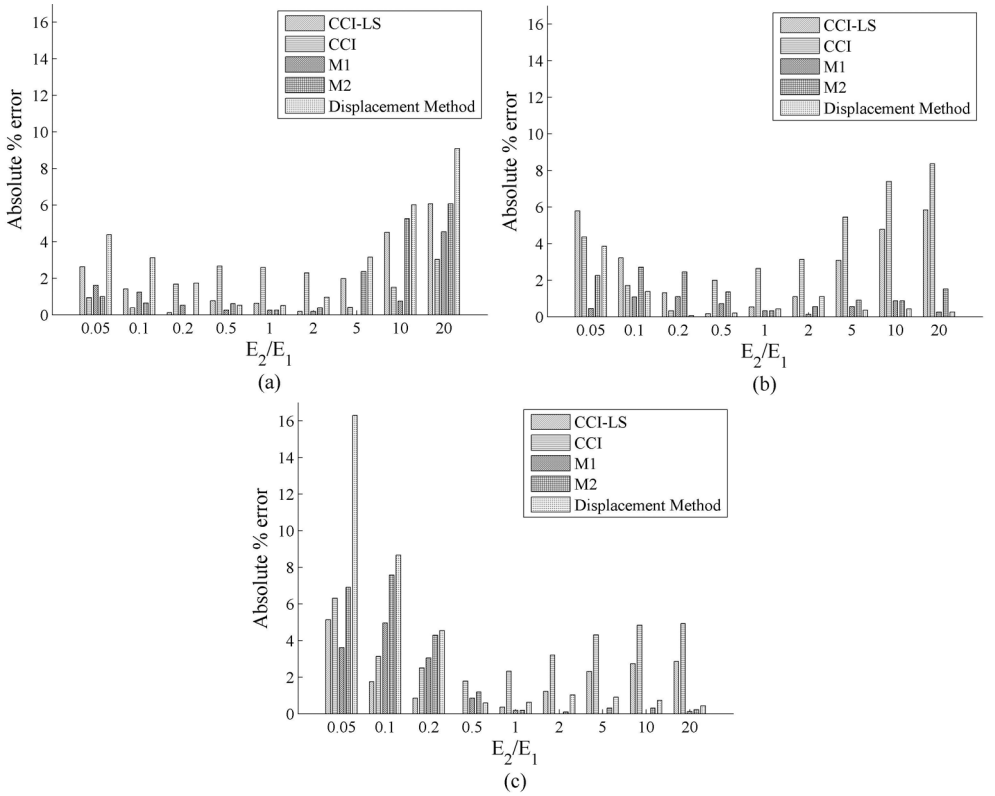


Figure 15. Absolute % error for (a) a/w = 0·45 (b) a/w = 0·5 (c) a/w = 0·55.

Table 6, Table 7 and Table 8 (Appendix C) show normalised Mode I SIFs obtained for various ratios. The results are compared with Ref. 8. The SIFs obtained by CCI-LS using XEFG method are satisfactory and compare closely with the results based on M-integral results. The following are the e_r of SIFs, for different a/w ratios, using various methods: –5·84% to 6·06% by CCI-LS, –8·38% to 4·37% by CCI, 0·00% to 4·95% by M1 integral, 0·00% to 7·57% by M2 integral and 0·03% to 16·32% by displacement method. Local smoothing scheme improves the results obtained by CCI. The SIFs obtained by displacement method deviate at extreme ratios of E_2/E_1.

5.0 CONCLUDING REMARKS

This paper presented accurate modeling of functionally graded materials using the extended element free-Galerkin method. Additionally, many techniques of extracting SIFs are described including the application of direct crack closure integral (CCI). The classical CCI was combined with a local smoothing technique to improve the accuracy of the computed SIFs. The local smoothing scheme adopted was elaborated. In general, a virtual crack extension length between 0·01a and 0·03a, where a is the crack length, is recommended for CCI. The proposed technique has been tested with several benchmark cases featuring a wide range of material properties and loading. It performed consistently well when compared with results available in the literature. It can also be easily applied to crack propagation studies in FGMs.

https://doi.org/10.1017/S0001924000007636 Published online by Cambridge University Press

REFERENCES

1. MARIN, L. Numerical solution of the Cauchy problem for steady-state heat transfer in two dimensional functionally graded material, *Int J Solids and Structures*, 2005, **42**, pp 4338-51.
2. MORTENSEN, A. and SURESH, S. Functionally graded metals and metal-ceramic composites: Part 1 Processing, *Int Material Reviews*, 1995, **30**, pp 83-93.
3. CHERRADI, N., KAWASAKI, A. and GASIK, M. Worldwide trends in functional gradient materials research and development, *Composites Engineering*, 1994, **8**, pp 883-94.
4. NEUBRAND, A. and RODE, J. Gradient materials: An overview of a novel concept, *Zeitschrift Fur Metallkunde*, 1997, **88**, pp 358-71.
5. SHANMUGAVEL, P. and BHASKAR, G.B., CHANDRASEKARAN, M, MANI, P.S. AND SRINIVASAN, S.P. An overview of fracture analysis in functionally graded materials, *European J Scientific Research*, 2012, **68**, pp 412-439.
6. TILBROOK, M.T., MOON, R.J. and HOFFMAN, M. Finite element simulations of crack propagation in functionally graded material under flexural loading, *Engineering Fracture Mechanics*, 2005, **72**, pp 2444-67.
7. LI, C., ZOU, Z. and DUAN, Z. Stress intensity factors for functionally graded solid cylinders, *Engineering Fracture Mechanics*, 1999, **63**, pp 735-49.
8. KIM, J.H. and PAULINO, G.H. Finite element evaluation of mixed mode stress intensity factors in functionally graded materials, *Int J Numerical Methods in Engineering*, 2002, **53**, pp 1903–35.
9. MOËS, N., DOLBOW, J. and BELYTSCHKO, T. A finite element for crack growth without remeshing, *Int J Numerical Methods in Eng*, 1999, **46**, pp 131-150.
10. NGUYEN, V.P., RABCZUK T., BORDAS, S. and DUFLOT, M. Meshless methods: A review and computer implementation aspects, *Mathematica and Computers in Simulation*, 2008, **79**, pp 763-813.
11. COMI, C. and MARIANI, S. Extended finite element simulation of quasi-brittle fracture in functionally graded materials, *Computer Methods in Applied Mechanics and Eng*, 2007, **196**, pp 4013-4026.
12. BELYTSCHKO, T., GU, L. and LU, Y.Y. Fracture and crack growth by element-free Galerkin methods, *Modelling and Simulation Material Science Eng*, 1994, **2**, pp 519-534.
13. VENTURA, G., XU, J.X. and BELYTSCHKO, T. A vector level set method and new discontinuity approximations for crack growth by EFG, *Int J Numerical Methods in Eng*, 2002, **54**, pp 923-944.
14. CHING, H.K. and YEN, S.C. Meshless local Petrov-Galerkin analysis for 2d functionally graded elastic solids under mechanical and thermal loads, *Composites Part B: Engineering*, 2005, **36**, pp 223-240.
15. GILHOOLEY, D.F., XIAO, J.R., BATRA, R.C., MCCARTHY, M.A. and GILLESPIE, J.W. Two-dimensional stress analysis of functionally graded solids using the MLPG method with radial basis functions, *Computational Materials Science*, 2008, **41**, pp 467-481.
16. RAO, B.N. and RAHMAN, S. Mesh-free analysis of cracks in isotropic functionally graded materials, *Engineering Fracture Mechanics*, 2003, **70**, pp 1–27.
17. DELALE, F. and ERDOGAN, F. The crack problem for a nonhomogeneous plane, *J Applied Mechanics*, 1983, **50**, pp 609–614.
18. ERDOGAN, F. Stress intensity factors, *J Applied Mechanics*, 1983, **50**, pp 992–1002.
19. EISCHEN, J.W. Fracture of nonhomogeneous materials, *Int J of Fracture*, 1987, **34**, pp 3–22.
20. CHAN, S.K., TUBA, I.S. and WILSON, W.K. On the finite element method in linear fracture mechanics, *Engineering Fracture Mechanics*, 1970, **30**, pp 227–231.
21. WATWOOD, V.B. The finite element method for prediction of crack behaviour, *Nuclear Engineering and Design*, 1969, **11**, pp 323–332.
22. RICE, J.R. A path independent integral and the approximate analysis of strain concentration by notches and cracks, *J Applied Mechanics*, 1968, **35**, pp 379-386.
23. RYBICKI, E.F. and KANNINEN, M.F. A finite element calculation of stress intensity factors by a modified crack closure integral, *Engineering Fracture Mechanics*, 1977, **9**, pp 931-938.
24. RAJU, I.S. Calculation of strain-energy release rates with higher order and singular finite elements, *Engineering Fracture Mechanic*s, 1987, **28**, pp 251-274.
25. MAITI, S.K. Finite element computation of crack closure integrals and stress intensity factors, *Engineering Fracture Mechanics*, 1992, **41**, pp 339-348.
26. YAU, J.F., WANG, S.S. and CORTEN, H.T. A mixed-mode crack analysis of isotropic solids using conservation laws of elasticity, *J Applied Mechanics*, 1980, **47**, pp 335–364.
27. KIM, J-H. and PAULINO, G.H. Consistent Formulations of the interaction integral method for fracture of functionally graded materials, *J Applied Mechanics*, 2005, **72**, pp 351–41.

https://doi.org/10.1017/S0001924000007636 Published online by Cambridge University Press

28. XUEPING, C., JUN, L. AND SHIRONG, L. EFG virtual crack closure technique for the determination of stress intensity factor, *Advanced Materials Research*, 2011, **250-253**, pp 3752-3758.
29. GUIAMATSIA, I., FALZON, B., DAVIES, G.A.O. and IANNUCCI, L. Element-free Galerkin modelling of composite damage, *Composites Science and Technology*, 2009, **69**, pp 2640-2648.
30. LANCASTER, P. and SALKAUSKAS, K. Surfaces generated by moving least square methods, *Mathematics of Computation*, 1981, **37**, pp 141-158.
31. MAITI, S.K., MUKHOPADHYAY, N.K. and KAKODKAR, A. Boundary element method based computation of stress intensity factor by modified crack closure integral, *Computational Mechanics*, 1997, **19**, pp 203–210.
32. DOLBOW, J.E. and GOSZ, M. On the computation of mixed-mode stress intensity factors in functionally graded materials, *Int J of Solids and Structures*, 2002, **39**, pp 2557–74.
33. ERDOGAN, F. and WU, B.H. The surface crack problem for a plate with functionally graded properties, *J Applied Mechanics*, 1997, **64**, pp 449–56.
34. CHEN, J., WU, L. and DU S. Element free Galerkin methods for fracture of functionally graded materials, *Key Engineering Materials*, 2000, **183–187**, pp 487–92.
35. DUNDURS, J. Edge-bonded dissimilar orthogonal elastic wedges, *ASME J Applied Mechanics*, 1969, **36**, pp 650-2.
36. Williams, M.L. On the stress distribution at the base of a stationary crack, *ASME J Applied Mechanics*, 1957, **24**, pp 109–14.
37. ANDERSON, T.L. *Fracture Mechanics, Fundamentals and Applications*, Second edition, 1995, CRC, New York, USA.

APPENDIX A

The auxiliary state is 2D Williams'[36] asymptotic crack tip solution[37] for stress and displacement. The auxiliary stress fields are given by:

$$\sigma_{11}^{aux} = \frac{1}{\sqrt{2\pi r}}\left\{K_I^{aux}\,\mathrm{Cos}\frac{\theta}{2}\left(1-\mathrm{Sin}\frac{\theta}{2}\mathrm{Sin}\frac{3\theta}{2}\right)-K_{II}^{aux}\,\mathrm{Sin}\frac{\theta}{2}\left(2+\mathrm{Cos}\frac{\theta}{2}\mathrm{Cos}\frac{3\theta}{2}\right)\right\} \quad \ldots (36)$$

$$\sigma_{22}^{aux} = \frac{1}{\sqrt{2\pi r}}\left\{K_I^{aux}\,\mathrm{Cos}\frac{\theta}{2}\left(1+\mathrm{Sin}\frac{\theta}{2}\mathrm{Sin}\frac{3\theta}{2}\right)+K_{II}^{aux}\,\mathrm{Sin}\frac{\theta}{2}\mathrm{Cos}\frac{\theta}{2}\mathrm{Cos}\frac{3\theta}{2}\right\} \quad \ldots (37)$$

$$\sigma_{12}^{aux} = \frac{1}{\sqrt{2\pi r}}\left\{K_I^{aux}\,\mathrm{Cos}\frac{\theta}{2}\mathrm{Sin}\frac{\theta}{2}\mathrm{Cos}\frac{3\theta}{2}+K_{II}^{aux}\,\mathrm{Cos}\frac{\theta}{2}\left(1-\mathrm{Sin}\frac{\theta}{2}\mathrm{Sin}\frac{3\theta}{2}\right)\right\} \quad \ldots (38)$$

The auxiliary displacements are given by

$$u_1^{aux} = \frac{1}{2\mu}\sqrt{\frac{r}{2\pi}}\left\{K_I^{aux}\,\mathrm{Cos}\frac{\theta}{2}\left(\kappa\text{-}1+2\mathrm{Sin}^2\frac{\theta}{2}\right)+K_{II}^{aux}\,\mathrm{Sin}\frac{\theta}{2}\left(\kappa+1+2\mathrm{Cos}^2\frac{\theta}{2}\right)\right\} \quad \ldots (39)$$

$$u_2^{aux} = \frac{1}{2\mu}\sqrt{\frac{r}{2\pi}}\left\{K_1^{aux}\,\mathrm{Sin}\frac{\theta}{2}\left(\kappa+1\text{-}2\mathrm{Cos}^2\frac{\theta}{2}\right)+K_{II}^{aux}\,\mathrm{Cos}\frac{\theta}{2}\left(\kappa\text{-}1\text{-}2\mathrm{Sin}^2\frac{\theta}{2}\right)\right\} \quad \ldots (40)$$

https://doi.org/10.1017/S0001924000007636 Published online by Cambridge University Press

APPENDIX B

Table 4
Mode I SIFs for edge crack subjected to constant tensile traction

		Normalised mode I SIF						
a/w	η	Ref. 33	Ref. 34	CCI-LS	CCI	M1	M2	Displacement method
0·2	0·1	1·297	1·32	1·293	1·267	1·322	1·301	1·286
				–0·31%	–2·31%	1·93%	0·31%	–0·85%
	0·2	1·396	1·419	1·391	1·363	1·417	1·4	1·388
				–0·36%	–2·36%	1·50%	0·29%	–0·57%
	5	1·132	1·162	1·133	1·109	1·147	1·153	1·138
				0·09%	–2·03%	1·33%	1·86%	0·53%
	10	1·002	1·032	1·005	0·983	1·016	1·025	1·01
				0·30%	–1·90%	1·40%	2·30%	0·80%
0·3	0·1	1·864	1·865	1·865	1·83	1·866	1·83	1·85
				0·38%	–1·51%	0·43%	–1·51%	–0·43%
	0·2	1·85	1·849	1·849	1·814	1·844	1·818	1·838
				0·49%	–1·41%	0·22%	–1·20%	–0·11%
	5	1·37	1·39	1·385	1·357	1·364	1·38	1·384
				1·09%	–0·95%	–0·44%	0·73%	1·02%
	10	1·229	1·25	1·245	1·219	1·223	1·244	1·245
				1·30%	–0·81%	–0·49%	1·22%	1·30%
0·4	0·1	2·57	2·559	2·575	2·531	2·565	2·502	2·561
				0·19%	–1·52%	–0·19%	–2·65%	–0·35%
	0·2	2·444	2·449	2·46	2·418	2·441	2·399	2·449
				0·65%	–1·06%	–0·12%	–1·84%	0·20%
	5	1·748	1·775	1·777	1·743	1·732	1·761	1·774
				1·66%	–0·29%	–0·92%	0·74%	1·49%
	10	1·588	1·615	1·617	1·585	1·57	1·608	1·614
				1·83%	–0·19%	–1·13%	1·26%	1·64%
0·5	0·1	3·57	3·521	3·539	3·49	3·557	3·453	3·539
				–0·87%	–2·24%	–0·36%	–3·28%	–0·87%
	0·2	3·327	3·323	3·336	3·288	3·337	3·268	3·336
				0·27%	–1·17%	0·30%	–1·77%	0·27%
	5	2·366	2·413	2·411	2·369	2·355	2·406	2·409
				1·90%	0·13%	–0·46%	1·69%	1·82%
	10	2·176	2·223	2·22	2·181	2·158	2·225	2·219
				2·02%	0·23%	–0·83%	2·25%	1·98%
0·6	0·1	5·188	5·073	5·012	4·961	5·078	4·906	5·05
				–3·39%	–4·38%	–2·12%	–5·44%	–2·66%
	0·2	4·761	4·786	4·725	4·672	4·758	4·65	4·755
				–0·76%	–1·87%	–0·06%	–2·33%	–0·13%
	5	3·445	3·574	3·516	3·465	3·439	3·526	3·524
				2·06%	0·58%	–0·17%	2·35%	2·29%
	10	3·212	3·337	3·282	3·232	3·188	3·306	3·287
				2·18%	0·62%	–0·75%	2·93%	2·33%

https://doi.org/10.1017/S0001924000007636 Published online by Cambridge University Press

Table 5
Mode I SIFs for edge crack subjected to linear tensile traction

		Normalised mode I SIF						
a/w	**η**	**Ref. 33**	**Ref. 8**	**CCI-LS**	**CCI**	**M1**	**M2**	**Displacement method**
0·2	0·1	1·904	1·888	1·886	1·85	1·905	1·878	1·892
				–0·95%	–2·84%	0·05%	–1·37%	–0·63%
	0·2	1·595	1·588	1·588	1·557	1·605	1·587	1·583
				–0·44%	–2·38%	0·63%	–0·50%	–0·75%
	5	0·687	0·687	0·692	0·677	0·701	0·703	0·696
				0·73%	–1·46%	2·04%	2·33%	1·31%
	10	0·565	0·565	0·571	0·559	0·579	0·582	0·575
				1·06%	–1·06%	2·48%	3·01%	1·77%
0·3	0·1	1·886	1·864	1·879	1·847	1·866	1·830	1·886
				–0·37%	–2·07%	–1·06%	–2·97%	0·00%
	0·2	1·612	1·601	1·617	1·588	1·604	1·581	1·622
				0·31%	–1·49%	–0·50%	–1·92%	0·62%
	5	0·778	0·790	0·79	0·775	0·778	0·786	0·792
				1·54%	–0·39%	0·00%	1·03%	1·80%
	10	0·659	0·659	0·672	0·658	0·661	0·671	0·673
				1·97%	–0·15%	0·30%	1·82%	2·12%
0·4	0·1	1·978	1·943	1·966	1·936	1·949	1·901	1·979
				–0·61%	–2·12%	–1·47%	–3·89%	0·05%
	0·2	1·721	1·706	1·729	1·701	1·709	1·679	1·738
				0·46%	–1·16%	–0·70%	–2·44%	0·99%
	5	0·924	0·924	0·942	0·924	0·918	0·933	0·944
				1·95%	0·00%	–0·65%	0·97%	2·16%
	10	0·804	0·804	0·823	0·807	0·799	0·817	0·824
				2·36%	0·37%	–0·62%	1·62%	2·49%
0·5	0·1	2·215	2·145	2·173	2·146	2·177	2·114	2·2
				–1·90%	–3·12%	–1·72%	–4·56%	–0·68%
	0·2	1·953	1·925	1·952	1·927	1·948	1·908	1·973
				–0·05%	–1·33%	–0·26%	–2·30%	1·02%
	5	1·152	1·158	1·182	1·163	1·155	1·179	1·188
				2·60%	0·95%	0·26%	2·34%	3·13%
	10	1·035	1·035	1·058	1·04	1·029	1·06	1·062
				2·22%	0·48%	–0·58%	2·42%	2·61%
0·6	0·1	2·717	2·553	2·582	2·559	2·611	2·523	2·633
				–4·97%	–5·82%	–3·90%	–7·14%	–3·09%
	0·2	2·404	2·341	2·371	2·348	2·384	2·327	2·413
				–1·37%	–2·33%	–0·83%	–3·20%	0·37%
	5	1·56	1·561	1·593	1·571	1·558	1·597	1·607
				2·12%	0·71%	–0·13%	2·37%	3·01%
	10	1·429	1·429	1·46	1·439	1·42	1·471	1·471
				2·17%	0·70%	–0·63%	2·94%	2·94%

https://doi.org/10.1017/S0001924000007636 Published online by Cambridge University Press

APPENDIX C

Table 6
Normalised mode I SIF for TPB specimen with $a/w = 0{\cdot}45$

	Normalised mode I SIF						
E_2/E_1	Ref. 8	Ref. 16 CCT	CCI–LS	CCI	M1	M2	Displacement method
0·05	33·04	32·99	33·91	33·35	33·57	33·37	34·49
			2·63%	0·94%	1·60%	1·00%	4·40%
0·1	23·47	23·61	23·80	23·38	23·76	23·62	24·20
			1·41%	–0·38%	1·24%	0·64%	3·11%
0·2	17·36	17·28	17·38	17·07	17·45	17·36	17·66
			0·12%	–1·67%	0·52%	0·00%	1·73%
0·5	11·65	11·45	11·56	11·34	11·62	11·58	11·71
			–0·77%	–2·66%	–0·26%	–0·60%	0·52%
1	8·13	7·96	8·08	7·92	8·11	8·11	8·17
			–0·62%	–2·58%	–0·25%	–0·25%	0·44%
2	5·24	5·15	5·23	5·12	5·23	5·26	5·29
			–0·19%	–2·29%	–0·19%	0·38%	0·87%
5	2·54	2·51	2·59	2·53	2·54	2·60	2·62
			1·97%	–0·39%	0·00%	2·36%	3·12%
10	1·33	1·31	1·39	1·35	1·32	1·40	1·41
			4·51%	1·50%	–0·75%	5·26%	6·19%
20	0·66	0·66	0·70	0·68	0·63	0·70	0·72
			6·06%	3·03%	–4·55%	6·06%	8·82%

https://doi.org/10.1017/S0001924000007636 Published online by Cambridge University Press

Table 7
Normalised mode I SIF for TPB specimen with $a/w = 0{\cdot}5$

	Normalised mode I SIF						
E_2/E_1	Ref. 8	Ref. 16 CCT	CCI-LS	CCI	M1	M2	Displacement method
0·05	31·12	31·53	32·92	32·48	30·98	30·42	32·32
			5·78%	4·37%	–0·45%	–2·25%	3·85%
0·1	23·92	23·96	24·69	24·33	23·66	23·27	24·25
			3·22%	1·71%	–1·09%	–2·72%	1·38%
0·2	18·32	18·36	18·56	18·26	18·12	17·87	18·33
			1·31%	–0·33%	–1·09%	–2·46%	0·03%
0·5	12·57	12·30	12·55	12·32	12·48	12·40	12·544
			–0·16%	–1·99%	–0·72%	–1·35%	–0·24%
1	9·47	9·21	9·42	9·22	9·44	9·44	9·51
			–0·53%	–2·64%	–0·32%	–0·32%	0·39%
2	7·32	7·34	7·24	7·09	7·31	7·36	7·40
			–1·09%	–3·14%	–0·14%	0·55%	1·02%
5	5·50	5·47	5·33	5·20	5·47	5·55	5·52
			–3·09%	–5·45%	–0·55%	0·91%	0·40%
10	4·59	4·62	4·37	4·25	4·55	4·63	4·57
			–4·79%	–7·41%	–0·87%	0·87%	–0·45%
20	3·94	3·99	3·71	3·61	3·93	4·00	3·93
			–5·84%	**–8·38%**	–0·25%	1·52%	–0·28%

Table 8
Normalised mode I SIF for TPB specimen with $a/w = 0{\cdot}55$

	Normalised mode I SIF						
E_2/E_1	Ref. 8	Ref. 16 CCT	CCI-LS	CCI	M1	M2	Displacement method
0·05	15·21	15·50	14·43	14·25	14·66	14·16	12·73
			–5·13%	–6·31%	–3·64%	–6·90%	–16·32%
0·1	13·73	13·40	13·49	13·30	13·05	12·69	12·54
			–1·75%	–3·13%	–4·95%	–7·57%	–8·68%
0·2	12·79	12·16	12·68	12·47	12·40	12·24	12·21
			–0·86%	–2·50%	–3·05%	–4·30%	–4·51%
0·5	11·76	11·29	11·76	11·55	11·66	11·62	11·69
			0·00%	–1·79%	–0·85%	–1·19%	–0·61%
1	11·15	10·85	11·11	10·89	11·13	11·13	11·22
			–0·36%	–2·33%	–0·18%	–0·18%	0·64%
2	10·62	10·44	10·49	10·28	10·62	10·63	10·73
			–1·22%	–3·20%	0·00%	0·09%	0·99%
5	9·96	9·93	9·73	9·53	9·96	9·99	10·05
			–2·31%	–4·32%	0·00%	0·30%	0·94%
10	9·50	9·59	9·24	9·04	9·50	9·53	9·57
			–2·74%	–4·84%	0·00%	0·32%	0·71%
20	9·12	9·27	8·86	8·67	9·11	9·14	9·16
			–2·85%	–4·93%	–0·11%	0·22%	0·38%

https://doi.org/10.1017/S0001924000007636 Published online by Cambridge University Press